PHOTONICS Research

Realizing fast temperature measurement and simulating Maxwell's demon with nearly nondestructive detection in cold atoms

Xin Wang,[1,2] Yuan Sun,[1,3] and Liang Liu[1,4]

[1]CAS Key Laboratory of Quantum Optics and Center of Cold Atom Physics, Shanghai Institute of Optics and Fine Mechanics, Chinese Academy of Sciences, Shanghai 201800, China
[2]Center of Materials Science and Optoelectronics Engineering, University of Chinese Academy of Sciences, Beijing 100049, China
[3]e-mail: yuansun@siom.ac.cn
[4]e-mail: liang.liu@siom.ac.cn

Received 5 January 2022; revised 19 May 2022; accepted 18 June 2022; posted 22 June 2022 (Doc. ID 453159); published 27 July 2022

Optical detection and manipulation of the thermal properties is an essential subject of cold atoms in the quantum era. For laser cooled alkali atoms, we have experimentally realized deterministic temperature measurement with time cost below 1 ms and effective filtering of colder atoms with temperature less than 1 μK, with the help of nearly nondestructive detection. The quick temperature measurement is accomplished by carefully resolving the diffusion dynamics of atoms with the information provided by a single probe laser pulse in the form of bucket detection, while suppressing the amplitude and phase noises of probe laser. The separation of colder atoms is attainable as the velocity differences of atoms translate into nontrivial position differences, when the diffusion sustains for a few tens of milliseconds. In particular, these efforts are based on a labeling process that distinguishes the cold atoms under study from the others by specific internal states, while the nearly nondestructive detection is implemented via driving a cycling transition with continuous optical pulses. Moreover, such a position-dependent labeling process can be further modified to become velocity-dependent, with which we have demonstrated a Maxwell's demon-type operation on cold atoms, as Maxwell's demon's intricate abilities can be understood as measuring the velocity of an individual particle and then performing feedback according to a straightforward dichotomy of the velocity value.

https://doi.org/10.1364/PRJ.453159

1. INTRODUCTION

Temperature is an essential topic in laser cooling of atoms [1,2], ions [3,4], molecules [5–7], solids [8–11], and cavity optomechanical systems [12–14]. The rapid development of quantum technologies with cold atom ensembles, including quantum precision measurement [15–17], quantum sensing [18], quantum simulation [19–21], and quantum information [22,23], raises emerging requirements for fast temperature measurement with minimal disturbance and an effective method of sorting out relatively colder atoms. However, the routine technique of time-of-flight (TOF) [24–27] is a destructive detection method that usually costs about a few tens to hundreds of milliseconds. Nondestructive thermometry has been developed for typical cold atom systems of optical molasses [28,29], optical dipole traps [30], and Bose–Einstein condensates (BECs) [31], and yet these methods still need significantly more than 1 ms data acquisition time in practice.

On the other hand, the idea of filtering colder atoms has profound connections with the concept of Maxwell's demon, which is an imagined creature with the ability of identifying particles with smaller velocities and subsequently separating them from the hotter ones [32]. Experiments with Maxwell's demon-type behavior have already been proposed and demonstrated in various systems [33–41]. For cold atoms, 1D quasi-single-velocity cooling [42] and one-way potential barriers for the optical dipole trap [43] have been realized. Nevertheless, generic Maxwell's demon-type operation of identifying atoms with smaller velocity values remains elusive in cold atom systems. Meanwhile, lower temperature often implies longer coherence time and better precision, especially in cold atom clock [44] and ultracold atom interferometry [45]; therefore, sorting out the relatively colder portion of a cold atom ensemble is not only theoretically interesting but also practically helpful.

In this paper, we first demonstrate deterministic measurement of temperature within less than 1 ms detection time and effective filtering of colder atoms with temperature less than 1 μK starting from an ensemble with about 20 μK. The essential procedure consists of a well calibrated labeling

operation of atoms and nearly nondestructive detection with continuous optical pulses, relying on the polarization control of the atoms' internal states and a cycling transition. Our method is compatible with various types of cold atom platforms, and here we choose isotropic laser cooling (ILC) [46–49] due to its advantage of generating cold atoms with nearly perfect isotropic thermal properties in all three dimensions. It is attainable to acquire information of temperature within 1 ms because the absorption change of probe laser is obviously distinguishable in theory even for cold atoms with very low temperature, when the signal-to-noise ratio is adequate. Then we move on to discuss sorting out the colder portion of labeled atoms, which amounts to mapping velocity distribution into spatial distribution over a few tens of milliseconds. Finally, we show that, by tuning the labeling process, whether the atom passing by the region of labeling lasers gets transferred to state will become dependent on its velocity. This almost reproduces the original thought experiment of a Maxwell's demon labeling the atoms according to their velocities, where the label is now instantiated in terms of the atomic internal states.

2. METHODS

The basic experimental setup is depicted in Fig. 1(a). The labeling lasers consist of the polarizing laser, which drives the

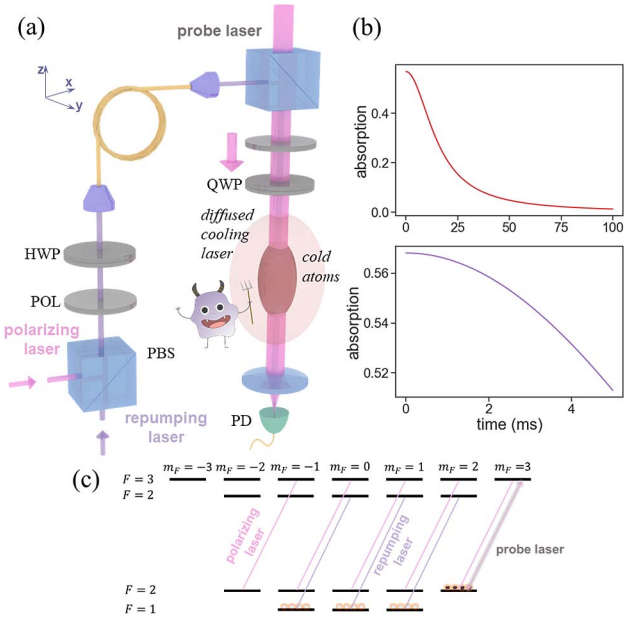

Fig. 1. (a) Schematic of the experiment. The cold atom ensemble is prepared by a uniformly diffused cooling laser. A polarizing beam splitter (PBS), polarizers (POL), and a half-wave plate (HWP) are employed to combine the polarizing laser and the repumping laser for the labeling process. A quarter-wave plate turns the labeling lasers and the probe laser into circular polarization. The probe laser propagates and eventually arrives at a photodetector (PD). The labeling lasers and probe laser are concentric and aligned along the direction of gravity. No bias magnetic field is required. (b) Theory curve of the absorption signal for cold atoms of 20 μK as the 2D temperature. (c) Relevant energy levels of ^{87}Rb D2 line for the experiment, including the details of Zeeman sub-states and laser polarizations for the nearly nondestructive detection method. The probe laser drives a cycling transition when the population is concentrated in $|F = 2, m_F = 2\rangle$.

population among $F = 2$ level toward $|F = 2, m_F = 2\rangle$, and the repumping laser, which drives the population from $F = 1$ to $F = 2$. They are of the same beam profile when they meet the cold atoms. By the end of laser cooling period, all the cold atoms will be sent to the $F = 1$ ground level. The successfully labeled atoms will then stay at $|F = 2, m_F = 2\rangle$ in contrast with the other ones. Here the population transfer relies on spontaneous emissions, and the labeling process typically requires several microseconds to a few tens of microseconds.

The density profile of labeled atoms will vary over time due to the diffusion related with their kinematic motions, and such a change can be revealed in the absorption signal of the probe laser in the form of bucket detection. The velocity distribution of these laser cooled atoms has been already identified as the Maxwell–Boltzmann distribution in previous experimental investigations [28,50], which corroborated the general theory of laser cooling [51]. Moreover, it is known that the cold atom density is reasonably uniform in the central region of ILC [52,53]. With these information as *a priori*, and taking the finite labeled area of the circular shape into consideration, an analytical formula describing the time-dependent absorption signal can be derived as

$$I_{\text{absorb}}(t) \simeq \mathcal{C} \times \frac{k_B T d^2}{m}\left(1 - \exp\left(-\frac{\xi\zeta}{\xi+\zeta}R_l^2\right)\right). \quad (1)$$

The details of derivation will be discussed later in Section 3.A. Here, $\mathcal{C}$ is an overall constant, k_B is the Boltzmann constant, m is the atomic mass, T is the 2D temperature of the x, y dimensions, d is the Gaussian diameter of the probe laser, R_l is the radius of labeled area in the x–y plane, and the parameters ξ, ζ are defined as

$$\xi = \frac{8}{d^2}, \qquad \zeta = \frac{m}{2k_B T t^2}. \quad (2)$$

A sample theory curve of Eq. (1) is shown in Fig. 1(b). We observe that the derivative is changing rapidly during the beginning few milliseconds, and this feature makes it possible to measure temperature on a time scale less than 1 ms. Namely, even for a small time duration, the bucket detection of the probe laser can effectively deduce the temperature, according to the density change due to the thermal motion of cold atoms.

ILC is usually realized in the form of generating cold atoms by diffuse reflection light [49,54–56]. Its operation requires neither the careful alignment of cooling lasers or the presence of magnetic gradient field, and it is known for the characteristics of compactness and robustness. The implementation of ILC usually relies on an all-optical structure with the surface of vacuum chamber coated with diffuse reflective material.

For our ILC process, the cooling lasers consist of the main cooling laser and the secondary repumping laser. The main cooling laser is typically red detuned by 20–25 MHz to the transition of $5^2S_{1/2}, F = 2 \leftrightarrow 5^2P_{3/2}, F = 3$, and the secondary repumping laser is tuned to the transition of $5^2S_{1/2}$, $F = 1 \leftrightarrow 5^2P_{3/2}, F = 2$. The power of the cooling laser is typically set at slightly above 100 mW, where we have experimentally observed that the saturation of the cold atom number starts to take place. Typically, the cold atom ensemble obtained via ILC is relatively dilute; therefore, it is vital to suppress the intensity and frequency noises of probe laser for the sake of a

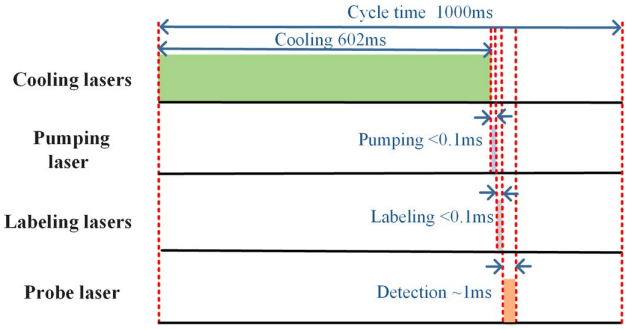

Fig. 2. Sample time sequence for our experiment of fast temperature measurement with nearly nondestructive detection. The pumping laser is resonant with the transition of $5^2S_{1/2}, F = 2 \leftrightarrow 5^2P_{3/2}, F = 2$.

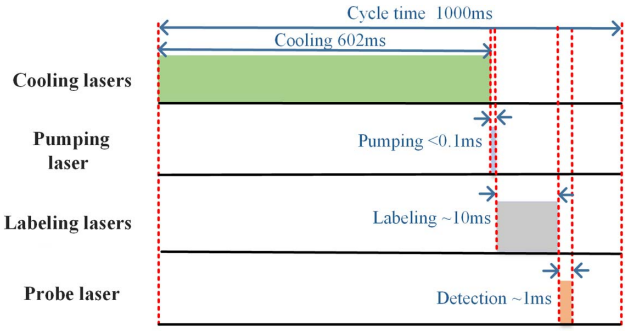

Fig. 3. Sample time sequence for our experiment of simulating Maxwell's demon in terms of velocity-dependent labeling. A mechanical shutter is employed to ensure the labeling lasers are stopped completely, such that we intentionally keep a waiting period up to several milliseconds at the end of cooling stage for it to stabilize, which is not necessary in theory. We omit this extra gap time in this graph.

good signal-to-noise ratio. With our choices of parameters, the cold atom density is typically on the order of 10^8 cm^{-3}, and the collision loss rate is on the order of 2 s^{-1}.

In order to realize the nearly nondestructive detection, it requires a proper time sequence of experiment. The sample time sequences of the fast temperature measurement and simulating Maxwell's demon experiments are demonstrated in Figs. 2 and 3, respectively. In particular, immediately after the cooling lasers are turned off, a pumping laser will optically pump all the cold atoms to the $F = 1$ ground level.

3. THEORY

A. Relation between the Time-Dependent Absorption Signal and Temperature

Here we discuss the detailed derivation of how to deduce the temperature of labeled cold atoms from the absorption signal of the probe laser in the form of bucket detection. In particular, the issue of finite labeling area determined by the labeling lasers will be specifically addressed.

First, we review the idealized case that the labeled atoms take the form of a thin line with zero width along the z direction. The Maxwell–Boltzmann distribution in 2D, with respect to the polar coordinate system, can be written as

$$f_2(v)\mathrm{d}v = \left(\frac{m}{2\pi k_B T}\right) 2\pi v \exp\left(-\frac{mv^2}{2k_B T}\right)\mathrm{d}v. \tag{3}$$

If we define an artificial proportionality constant $\eta > 0$ to convert the optical depth (OD) at point (x, y) to the density $n(x, y)$, then the transmission of probe laser $I_{\mathrm{total}}(t)$ can be calculated as

$$I_{\mathrm{total}}(t) = \int_0^\infty \mathrm{d}r r \cdot I_p e^{-\frac{2r^2}{(d/2)^2}} \cdot \exp\left(-\eta \frac{1}{t^2} e^{-\frac{m(r/t)^2}{2k_B T}}\right), \tag{4}$$

with normalization in the value of

$$\int_0^{+\infty} \mathrm{d}r r \cdot I_p e^{-\frac{2r^2}{(d/2)^2}}. \tag{5}$$

Inevitably, the thin line description is oversimplified for the actual situation encountered in experimentation, especially during the beginning phase of a few milliseconds immediately after the labeling process. In order to take the finite labeling area into consideration, we assume a uniform physical density of the cold atoms near the central region, which is a reasonable thing to expect for ILC [46–49,52,53]. Then the absorption of the probe laser includes the contributions of cold atoms traveling from all possible originates within the effective labeling area. According to this viewpoint, the transmission can be calculated as

$$I_{\mathrm{total}}(t) \simeq \iint \mathrm{d}X\mathrm{d}Y I_p e^{-\frac{2(X^2+Y^2)}{(d/2)^2}} \cdot \exp\left(-\iint_S \mathrm{d}x\mathrm{d}y \eta \frac{1}{t^2} e^{-\frac{m}{2k_B T}\frac{(X-x)^2+(Y-y)^2}{t^2}}\right), \tag{6}$$

which can also be understood as a form of convolution based on Eq. (4). Here we can employ the approximation of $e^\epsilon \approx 1 + \epsilon$ for $\epsilon \ll 1$:

$$I_{\mathrm{total}}(t) \approx \iint \mathrm{d}X\mathrm{d}Y I_p e^{-\frac{2(X^2+Y^2)}{(d/2)^2}} \cdot \left(1 - \eta \frac{1}{t^2} \iint_S \mathrm{d}x\mathrm{d}y e^{-\frac{m}{2k_B T}\frac{(X-x)^2+(Y-y)^2}{t^2}}\right). \tag{7}$$

The above expression leaves us to evaluate an integral in the form of

$$\int_{-\infty}^{\infty} \mathrm{d}u \exp\left(-\frac{8}{d^2}u^2 - \frac{m}{2k_B T t^2}u^2 + \frac{m}{k_B T t^2}uu_0 - \frac{m}{2k_B T t^2}u_0^2\right). \tag{8}$$

As in Eq. (1), we adopt the two parameters ξ, ζ to simplify the notation, and then the value of Eq. (8) can be directly computed as

$$\frac{\sqrt{\pi}}{\sqrt{\xi + \zeta}} \exp\left(\left(\frac{\zeta^2}{\xi + \zeta} - \zeta\right)u_0^2\right). \tag{9}$$

Since Eq. (7) describes the transmitted light, and therefore in the polar coordinate system, the absorption of light is proportional to

$$\frac{1}{t^2} \cdot \frac{\pi}{\xi + \zeta} \cdot 2\pi \cdot \int_0^{R_l} r\mathrm{d}r \exp\left(\left(\frac{\zeta^2}{\xi + \zeta} - \zeta\right)r^2\right), \tag{10}$$

where R_l is the radius of the prescribed labeled region. With the above preparations, we eventually arrive at the following expression of Eq. (1), as stated previously in Section 2.

When Eq. (1) is employed in the fitting process to extract the value of temperature, typically it will only need two free parameters: constant and T. If the maximum absorption rate immediately after the labeling process is already known, then there exists only one free parameter T in the fitting process.

In Fig. 4, we show a few typical theory curves with emphasis put on the first few milliseconds immediately after the labeling process. From the behavior of curves associated with different temperature values, we observe that ~1 ms of data can yield a deterministic and reliable temperature measurement, as long as the signal-to-noise ratio is adequate. On the other hand, there exist a few factors that can influence the accuracy of Eq. (1). For example, the velocity distribution may deviate from the standard Maxwell–Boltzmann distribution, or the density of cold atoms in the labeling region can be non-uniform.

B. Filtering Out the Colder Part of Labeled Atoms

Once the labeling procedure is accomplished, the labeled atoms staying within the region defined by the probe laser become colder and colder as time elapses since the hotter atoms gradually leave the region. Such a process effectively behaves like filtering out the colder atoms.

Here we discuss the details about how to quantitatively describe such a process. As in the previous analysis, the derivations will be put under the 2D framework in the $(x$–$y)$ plane. Certainly the velocity distribution of the atoms staying in the confined region will not necessarily obey the status of an equilibrium state. Therefore, we would like to proceed with the concept of effective temperature T_e, defined in terms of the averaged kinetic energy. According to the experiment procedure, T_e is a function of time. A prerequisite is that the overall temperature value $\mathcal{T}$ at the beginning is already known.

With these preparations, we can express $T_e(t)$ as follows:

$$k_B T_e(t) \equiv \frac{1}{\mathrm{Norm}(\mathcal{T},t)} \iint_{S_p} \mathrm{d}X\mathrm{d}Y \times \iint_{S_l} \mathrm{d}x\mathrm{d}y \frac{1}{2} m \frac{(X-x)^2+(Y-y)^2}{t^2} e^{-\frac{m}{2k_B T}\frac{(X-x)^2+(Y-y)^2}{t^2}}, \tag{11}$$

with S_p, S_l representing the probe region and the labeling region, respectively. Correspondingly, the normalization $\mathrm{Norm}(\mathcal{T})$ is

$$\mathrm{Norm}(\mathcal{T},t) \equiv \iint_{S_p} \mathrm{d}X\mathrm{d}Y \iint_{S_l} \mathrm{d}x\mathrm{d}y e^{-\frac{m}{2k_B T}\frac{(X-x)^2+(Y-y)^2}{t^2}}, \tag{12}$$

where an essential and interesting criterion is that $T_e(0)$ will equal the value of $\mathcal{T}$.

In order to comply with the typical situation with circular symmetry, we can reformulate Eq. (11) into a format with specific individual integral limits in the polar coordinates. And, eventually, with the interpretations that X, Y, x, y are functions of $r_p, \theta_p, r_l, \theta_l$, we arrive at the following formula:

$$\begin{aligned} k_B T_e(t) = {} & \frac{1}{\mathrm{Norm}(\mathcal{T},t)} \times \frac{1}{2} m v_r^2 \times \int_0^{s_p} \mathrm{d}r_p \int_0^{2\pi} \mathrm{d}\theta_p \\ & \times \int_0^{s_l} \mathrm{d}r_l \int_0^{2\pi} \mathrm{d}\theta_l r_p r_l \frac{(X-x)^2+(Y-y)^2}{(v_r t)^2} \\ & \times \exp\left(-\frac{1}{2}\frac{T_r}{\mathcal{T}}\frac{(X-x)^2+(Y-y)^2}{(v_r t)^2}\right), \end{aligned} \tag{13}$$

where the relation of $k_B T_r = m v_r^2$ is used.

Although Eq. (13) cannot be further reduced to an analytical form, it can be evaluated by numerical integration methods, as we will show later in Section 4.

C. Velocity-Dependent Labeling Process

Here we discuss a few more theoretical details about simulating the Maxwell's demon thought experiment with the velocity-dependent labeling process.

The essence is to investigate the relation between averaged number of scattering events in the optical pumping process toward the destination state of $|F=2, m_F=+2\rangle$. In our experiment, the repumping laser and the polarizing laser are both of the right circular polarization. We make a few assumptions to simplify the calculations. The first is the one-way repumping performance in the process of $F=1 \to F=2$. Namely, when the population in $F=1$ level is excited, we postulate that the spontaneous emission only allows decaying to $F=2$. The second is the one-way polarizing performance in the process of moving population in $F=2$ level to $|F=2, m_F=+2\rangle$. Namely, when the population in $F=2$ level is interacting with the polarizing laser, we postulate again that the spontaneous emission only allows decay back to $F=2$ level.

Initially, the atomic population is evenly distributed among the three states: $|F=1, m_F=-1\rangle, |F=1, m_F=0\rangle,$

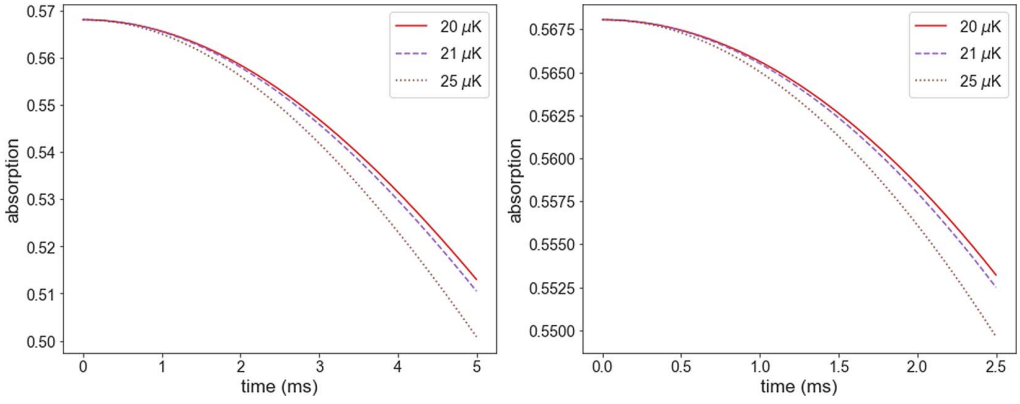

Fig. 4. Theory curves according to Eq. (1).

$|F=1,m_F=+1\rangle$. With the above assumptions, the optical pumping processes for these three different initial states are described as follows:

$$|F=1,m_F=-1\rangle:|F=1,m_F=-1\rangle \overset{\text{rep.}}{\Rightarrow} |F=2,m_F=0\rangle \overset{\text{pol.}}{\Rightarrow} |F=2,m_F=+1\rangle \overset{\text{pol.}}{\Rightarrow} |F=2,m_F=+2\rangle.$$

$$|F=1,m_F=0\rangle:|F=1,m_F=0\rangle \overset{\text{rep.}}{\Rightarrow} |F=2,m_F=+1\rangle \overset{\text{pol.}}{\Rightarrow} |F=2,m_F=+2\rangle.$$

$$|F=1,m_F=+1\rangle:|F=1,m_F=+1\rangle \overset{\text{rep.}}{\Rightarrow} |F=2,m_F=+2\rangle.$$

Therefore, in such a simplified picture, on average it takes one scattering event of the repumping laser and one scattering event of the polarizing laser to reach the destination of $|F=2,m_F=+2\rangle$.

On the other hand, a more rigorous approach needs to include the details of spontaneous emissions and the nuances of different Zeeman sub-states. The Monte Carlo wave function (MCWF) method serves well for this purpose, and we briefly discuss the basic formalism here. We begin with the equations of motion for the atomic wave functions without decay. According to the linkage structure of the atomic transitions that we have chosen, under the rotating wave approximation, the time evolution of the wave function can be expressed in terms of ordinary differential equations. For the wave function, we use the notation of $C_{l,j}$, with $l=g,e$ representing the states in the ground level of $5^2S_{1/2}$ and excited level of $5^2P_{3/2}$, respectively, and j representing the numbering of specific transitions. The detuning term is defined as $\delta=\omega_{\text{laser}}-\omega_{\text{atom}}$. The specifics are given in Tables 1 and 2.

Then, the ordinary equation system can be expressed in terms of

$$i\frac{\mathrm{d}}{\mathrm{d}t}\begin{bmatrix} C_{g,j} \\ C_{e,j} \end{bmatrix} = \begin{bmatrix} 0 & \frac{1}{2}\Omega_j \\ \frac{1}{2}\Omega_j^* & -\delta_j \end{bmatrix} \cdot \begin{bmatrix} C_{g,j} \\ C_{e,j} \end{bmatrix}, \tag{14}$$

just like a set of individual two-level atoms. The reference frame is set on the cold atom here; therefore, the atom sees time-dependent driving fields of $\Omega_p(t),\Omega_r(t)$ as the atom traveling through the repumping and polarizing lasers with Gaussian profile.

Next, the spontaneous emission can be treated as quantum jumps with the help of the pseudorandom number generators, according to the framework of MCWF method. The destination of spontaneous emission can be set as the randomized linear superposition of physically allowed states in the ground level, in order to better emulate the optical pumping effects. After running many such MCWF trajectories, the averaged numerical result will become a reasonable explanation of the velocity-dependent labeling process.

Table 1. Rabi Frequencies for the Transitions Associated with the Repumping Laser in the Labeling Interaction Process[a]

j	$\lvert g,j\rangle$	$\lvert e,j\rangle$	Ω_j
1	$\lvert F=1,m_F=-1\rangle$	$\lvert F=2,m_F=0\rangle$	$\sqrt{\frac{1}{6}}\Omega_r$
2	$\lvert F=1,m_F=0\rangle$	$\lvert F=2,m_F=+1\rangle$	$\sqrt{\frac{1}{2}}\Omega_r$
3	$\lvert F=1,m_F=+1\rangle$	$\lvert F=2,m_F=+2\rangle$	Ω_r

[a]The Rabi frequency Ω_r is defined with respect to the relatively strongest transition of $|5^2S_{1/2},F=1,m_F=+1\rangle\leftrightarrow|5^2P_{3/2},F'=2,m_F=+2\rangle$.

Table 2. Rabi Frequencies for the Transitions Associated with the Polarizing Laser in the Labeling Interaction Process[a]

j	$\lvert g,j\rangle$	$\lvert e,j\rangle$	Ω_j
4	$\lvert F=2,m_F=-2\rangle$	$\lvert F=3,m_F=-1\rangle$	$\sqrt{\frac{1}{15}}\Omega_p$
5	$\lvert F=2,m_F=-1\rangle$	$\lvert F=3,m_F=0\rangle$	$\sqrt{\frac{1}{5}}\Omega_p$
6	$\lvert F=2,m_F=+0\rangle$	$\lvert F=3,m_F=+1\rangle$	$\sqrt{\frac{2}{5}}\Omega_p$
7	$\lvert F=2,m_F=+1\rangle$	$\lvert F=3,m_F=+2\rangle$	$\sqrt{\frac{2}{3}}\Omega_p$
8	$\lvert F=2,m_F=+2\rangle$	$\lvert F=3,m_F=+3\rangle$	Ω_p

[a]The Rabi frequency Ω_p is defined with respect to the relatively strongest transition of $|5^2S_{1/2},F=2,m_F=+2\rangle\leftrightarrow|5^2P_{3/2},F'=3,m_F=+3\rangle$.

4. RESULTS AND DISCUSSION

A typical experimental result is shown in Fig. 5, where the absorption signal is collected from a single continuous pulse of probe laser and the data point is recorded every 5 μs. Here, the radius of labeled area R_l is 0.48 mm. Due to the cycling transition, the internal states of the labeled atoms virtually do not change during detection on the order of milliseconds, as the probe laser is kept at 0.2 μW with a Gaussian radius of 1.30 mm. Frequency and power fluctuations of the probe laser significantly affect the signal-to-noise ratio. Here, the frequency stabilization is realized by saturation absorption spectroscopy (SAS) with external modulation, and the power stabilization is implemented by a Brockton Electro-Optics LPC series power

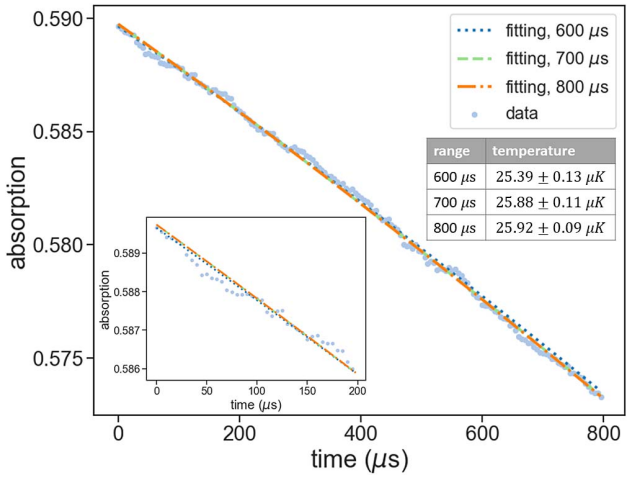

Fig. 5. Obtain temperature from a single trace of experimental data, costing less than 1 ms. The inset shows the details of the first 200 μs. This probe laser pulse starts at 3.3 ms after the labeling process, mostly because of waiting for the mechanical shutter of labeling lasers to fully close. The method of trust region reflective is employed for the fitting.

controller. The 2D temperature is determined by fitting to Eq. (1), where the outcome values based on data of different time durations are shown in Fig. 5.

In order to verify our description of the dynamics, especially on a relatively large time scale, we further carry out the experiment with two short probe pulses separated by tens of milliseconds. In fact, such a dual-pulse measurement is made possible by the nearly nondestructive detection, as the first probe pulse does not disturb the labeled cold atoms or cause excessive heating. In Fig. 6, we demonstrate a representative result, together with a fitting to the overall data according to Eq. (1). We observe that the global fitting curve agrees well with the experimental data locally for both pulses, which supports the accuracy of temperature measurement with less than 1 ms data taken very soon after the labeling operation. We repeat this type of dual-pulse experiment multiple times with different initial temperatures ranging from 10 μK to 30 μK, and similar to the situation of Fig. 6, the outcomes are consistent with our anticipations.

Moreover, we can vary the delay times in the dual-pulse experiment. In Fig. 6, we have intentionally presented the experimental result with a relatively long delay time in order to show the effects of velocity filtering. On the other hand, we can certainly choose a shorter delay time, as shown in Fig. 7. Again, we observe that the global fitting curve agrees well with the experimental data.

In the derivation of Eq. (1), the kinematic motions of labeled cold atoms along the z dimension are neglected, and the outcomes of dual-pulse experiment indicate that this assumption is reasonable, as long as the labeled atoms do not hit the wall of vacuum system. Furthermore, these outcomes imply that the velocity distribution is indeed close to Maxwell–Boltzmann, as expected. We also observe that Eq. (1) adequately describes the interaction between the probe laser and the labeled cold atoms on a time scale from ∼1 ms to ∼100 ms as, in the fitting of Figs. 5–7, the only two free parameters are T and $\mathcal{C}$.

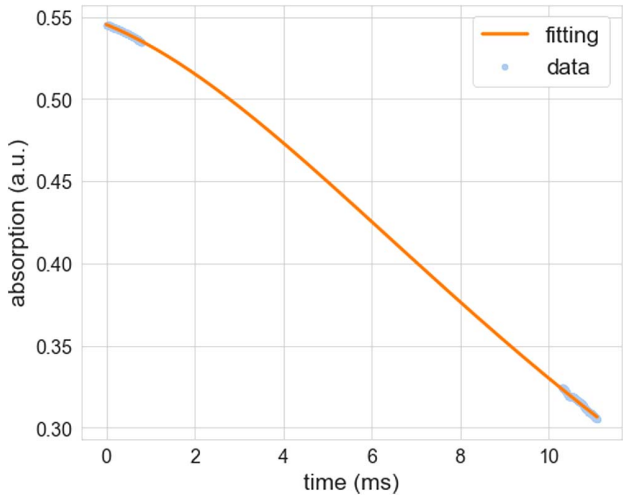

Fig. 7. Result of dual-pulse experiment with a relatively short time delay between the two probe pulses.

On the other hand, the result of Fig. 6 can be interpreted from an alternative viewpoint that the hotter atoms quickly leave the region defined by the probe laser while the cooler atoms tend to stay longer. Therefore, the dual-pulse experiment can behave as an effective method to filter out the colder part of the labeled atoms, where the nondestructive detection serves an indicator of the filtering process. As time elapses, the velocities of leftover labeled atoms gradually deviate from the Maxwell–Boltzmann distribution while the idea of thermal equilibrium apparently does not apply; therefore, the concept of temperature requires careful clarifications. Here we calculate the temperature as the averaged kinematic energies of the x, y dimensions. We focus on the labeled atoms within the disk area of probe laser's Gaussian diameter d and compute the temperature of residual cold atoms as a function of time, as in Fig. 8. It shows that, after about 74 ms delay from labeling, the 2D

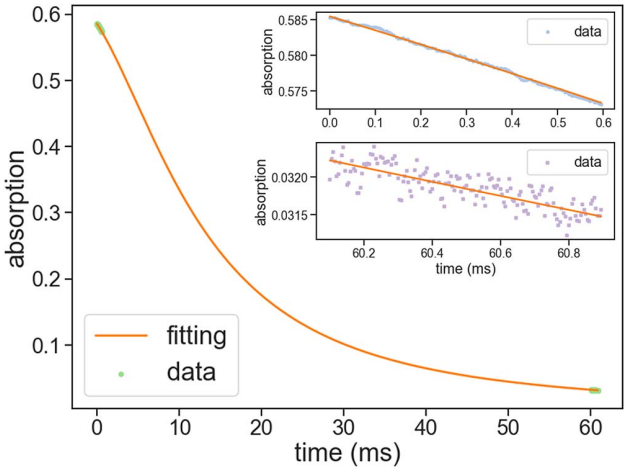

Fig. 6. Result of dual-pulse experiment, obtained from a single experimental trial. The inset shows the detailed data of the two pulses, respectively. Here the radius of labeled area R_l is 0.64 mm, and the first probe pulse starts at 4 ms after the labeling process. The overall fitted temperature is 24.83 μK with uncertainties less than 0.1 μK.

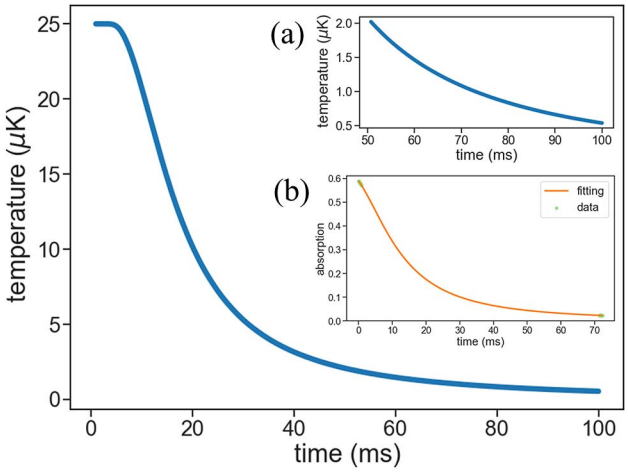

Fig. 8. Theory curve that describes the filtering of colder atoms in terms of 2D temperature, with $R_l = 0.64$ mm and $d = 2.60$ mm. (a) Details of the tail part. (b) Experimental dual-pulse detection result with initial temperature about 25.0 μK, also starting at 4 ms after labeling.

temperature of residual atoms drops below 1 μK. Following this observation, we perform a dual-pulse experiment with adequate time delay, and the result clearly demonstrates that the sub-μK portion of the labeled cold atoms has been filtered out, as presented in Fig. 8(b).

Our implementation of filtering has been limited to the 2D setting. If a fully 3D result is wanted, then extra operations need be applied to the dynamics of z dimension. We discuss several possibilities here. For the case of the micro-gravity environment [44,45], the diffusion of cold atoms can be regarded as isotropic; therefore, the task is to break the uniformity of the labeling process along the z direction. This can be implemented by a magnetic gradient or an extra ac Stark shift laser, which ensures that resonance only occurs around a fixed z point. For the case of on-ground environment with the presence of gravity, the situation is more complicated due to the additional overall velocity $-gt$ gained over delay time t, which can be resolved by launching the atoms initially at gt via moving optical molasses.

Next, we turn our attention back to the labeling process. Previously, its role was limited to quickly optically pumping the cold atoms within a prescribed region to the specific target state $|F = 2, m_F = 2\rangle$. On the other hand, if the intensity of the labeling lasers is intentionally kept at a relatively low level, then the atoms need a few milliseconds or more of interaction time to be properly sent to the target state. Therefore, when the atoms travel through the finite area of labeling lasers in x–y plane, the probability of labeling becomes dependent on their velocities, as shown in Fig. 9(a). Approximately speaking, the slow atoms will go to $|F = 2, m_F = 2\rangle$ while the fast atoms stay at $F = 1$. In the original version of Maxwell's demon thought experiment, the fast and slow atoms are separated in the spatial degree of freedom, namely that they are sent to two different compartments. In our experiment, the separation is realized in the internal degrees of freedom, namely $F = 1$ and $F = 2$ levels. Despite this subtle difference, if a translation to the original version is desired, then it is possible to implement a state-dependent optical force in the form of optical dipole trap to mechanically separate the fast and slow atoms.

We estimate the velocity dependence of such labeling processes in a simplified way. On average, it takes one scattering event of the repumping laser and one scattering event of the polarizing laser to reach $|F = 2, m_F = 2\rangle$, assuming they drive a one-way process of $F = 1 \to F = 2$. We proceed with ample polarizing laser power and investigate the relation between the labeling process and the repumping laser. We neglect the subtle differences of Clebsch–Gordon coefficients in Rabi frequency Ω, and then the excited level population is $\rho_{ee}(\delta) = (s_0/2)(1 + s_0 + (2\delta/\gamma)^2)^{-1}$, with $s_0 \equiv 2|\Omega|^2/\gamma^2$. The averaged time for one scattering event, or characteristic time τ_m, can be expressed as $\tau_m = 1/(\gamma\rho_{ee})$. Take the atom traveling through the center of labeling lasers as an example. As an idealization, we use the top hat profile of radius $0.5w_l$ and intensity $2\exp(-0.5)P/(\pi w_l^2)$ to model the repumping laser of Gaussian radius w_l and power P. Then we may define a characteristic velocity v_m as the maximum speed that can be properly labeled, in terms of $v_m = w_l/\tau_m$.

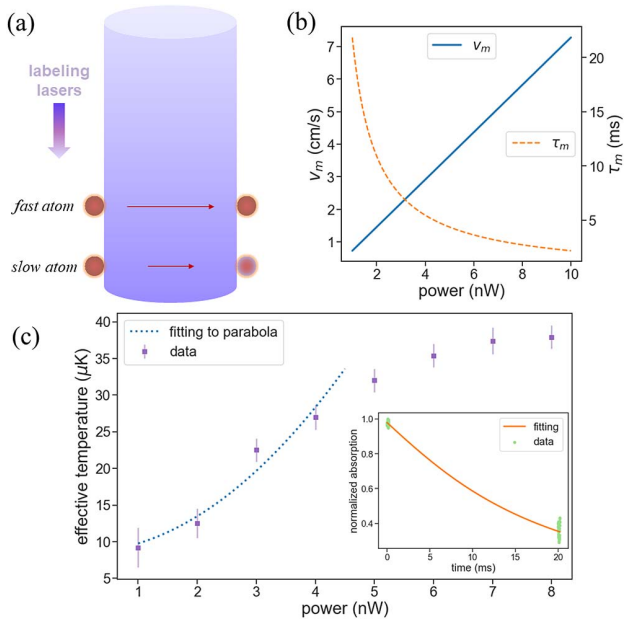

Fig. 9. (a) Cartoon of atoms traveling through the region of labeling lasers, which leads to velocity-dependent labeling. (b) Relation between τ_m, v_m and repumping laser power. If the Clebsch–Gordon coefficients or the actual Gaussian beam profile is included into consideration, the result does not change significantly. (c) Result of the velocity-dependent labeling experiment, showing the ability to distinguish fast and slow atoms in the sense of Maxwell's demon through experiment. From the viewpoint of classical mechanics, this is analogous to the case of separating hotter and colder atoms into isolated $V/2$ segments, respectively, from an original containment of volume V. If we set all the labeling times at 10 ms, the behavior is similar. The inset shows the details of 2 nW data point, which is smoothed with a rolling average of every five points.

The relation between τ_m, v_m and P is shown in Fig. 9(b) for $w_l = 0.318$ mm and $\delta = 2\pi \times 24$ MHz. Other atoms with off-center trajectories will need even lower velocities to acquire enough time to reach $|F = 2, m_F = 2\rangle$. From the viewpoint of Maxwell's demon thought experiment, here the demon's ability of judging velocity comes from $\Delta x/\Delta t$, where Δx represents the size of interaction area and Δt represents the minimal time required to complete optical pumping in the average sense.

We proceed with measurements according to the above discussions, with a larger cooling laser power such that the atoms begin with 2D temperature much higher than that of Fig. 5. In particular, we set the labeling interaction time as τ_m according to Fig. 9(b) for different laser powers, with two subsequent probe pulses separated by about 20 ms. The different interaction times serve partly for the purpose of avoiding large variances in the numbers of labeled atoms over multiple labeling processes. Certainly, the velocity distribution of labeled atoms here does not necessarily obey Maxwell–Boltzmann distribution. Nevertheless, in order to interpret the results, we use Eq. (1) to fit for a value of effective temperature from the experimental data, and a typical outcome is shown in Fig. 9(c). We observe that the velocity-dependent labeling effect is realized, and the effective temperature virtually stays the same when the repumping laser power increases above a threshold.

Several factors contribute to the imperfections of this result. The modeling of the physical process is oversimplified; for example, the time evolution of the atoms can be analyzed in a more thorough form to include all the Zeeman sub-states. The interpretation of experimental data can be refined to include more details of the labeled atoms' kinematics. Experimentally, the polarization quality of label lasers can be improved while the noise associated with probe laser pulses can be further suppressed.

ILC leads to relatively dilute cold atom gases; therefore, we have carefully suppressed the intensity and frequency noises of probe laser in order to obtain a good signal-to-noise ratio, which is vital in the temperature measurement process as can be seen in discussions of Section 3. While we have demonstrated so far that our experiments behave for such a dilute gas OD on the order of 1 or even less, we have also set up experimental tests to verify that it works well for cold atom ensembles with much higher density, and in particular with respect to a high density cold atom ensemble prepared via 3D magneto-optical trap (MOT). The preliminary testing results suggest that we have obtained essentially the same kind of behavior in the outcome. In particular, a cold atom ensemble with higher OD reduces the requirements on the probe laser.

In fact, since the velocity of cold atoms almost stays unchanged during the process, the analysis of entropy can be established by paying attention only to the internal degrees of freedom. In such a simplified picture, we assume that here exist two different states of $|0\rangle$ and $|1\rangle$, and all the atoms are in the same quantum state to begin with. After the interaction process, the hotter atoms are in state $|1\rangle$, and the colder atoms are in state $|0\rangle$. For one cold atom participating in such a velocity-dependent labeling process, the information entropy changes in the amount of exactly 1 bit. Moreover, Landauer's principle dictates the minimum work required to erase it. The second law of thermodynamics requires the overall entropy of an entire system to increase over time. As the case of laser cooling, the entire system consists of the atoms and the optical field [57,58]. Similarly, for our experiment, the highly ordered optical fields of the labeling lasers are scattered into disordered states during the interaction leading to velocity-dependent labeling. In other words, the entropy increase of the entire system takes place mostly in terms of the spontaneous emissions. This observation also implies that our experiment is connected with the entropy exchange problem of laser cooling, although virtually no reduction is made to the kinetic energy of cold atoms here.

5. CONCLUSION

In summary, we propose and demonstrate sub-millisecond temperature measurement of labeled cold atoms by a single continuous probe pulse in the form of nearly nondestructive detection. We further utilize this method to show that it is possible to filter out the sub-μK part from labeled atoms of tens of μK in a straightforward way, evaluated in the x, y dimensions. Moreover, we have realized a velocity-dependent labeling effect by adjusting the labeling process, in the style of Maxwell's demon thought experiment. Our experiment does not require subtle quantum coherence effects or delicate quantum manipulation techniques. While we focus on the 2D properties in this work, extension to a full 3D approach is attainable with reasonable upgrades.

Funding. National Natural Science Foundation of China (92165107); National Key Research and Development Program of China (2016YFA0301504).

Acknowledgment. The authors gratefully acknowledge support from the National Natural Science Foundation of China, the National Key R&D Program of China, and the Chinese Academy of Sciences, the China Manned Space Engineering Office. The authors also thank Ning Chen, Yanling Meng, Peng Xu, and Xiaodong He for helpful discussions.

Disclosures. The authors declare no conflicts of interest.

Data Availability. Data underlying the results presented in this paper are not publicly available at this time but may be obtained from the authors upon reasonable request.

REFERENCES

1. W. D. Phillips and H. Metcalf, "Laser deceleration of an atomic beam," Phys. Rev. Lett. **48**, 596–599 (1982).
2. S. Chu, L. Hollberg, J. E. Bjorkholm, A. Cable, and A. Ashkin, "Three-dimensional viscous confinement and cooling of atoms by resonance radiation pressure," Phys. Rev. Lett. **55**, 48–51 (1985).
3. F. Diedrich, J. C. Bergquist, W. M. Itano, and D. J. Wineland, "Laser cooling to the zero-point energy of motion," Phys. Rev. Lett. **62**, 403–406 (1989).
4. J. I. Cirac and P. Zoller, "Quantum computations with cold trapped ions," Phys. Rev. Lett. **74**, 4091–4094 (1995).
5. I. Kozyryev, L. Baum, K. Matsuda, B. L. Augenbraun, L. Anderegg, A. P. Sedlack, and J. M. Doyle, "Sisyphus laser cooling of a polyatomic molecule," Phys. Rev. Lett. **118**, 173201 (2017).
6. J. Lim, J. R. Almond, M. A. Trigatzis, J. A. Devlin, N. J. Fitch, B. E. Sauer, M. R. Tarbutt, and E. A. Hinds, "Laser cooled YbF molecules for measuring the electron's electric dipole moment," Phys. Rev. Lett. **120**, 123201 (2018).
7. L. Baum, N. B. Vilas, C. Hallas, B. L. Augenbraun, S. Raval, D. Mitra, and J. M. Doyle, "1D magneto-optical trap of polyatomic molecules," Phys. Rev. Lett. **124**, 133201 (2020).
8. R. I. Epstein, M. I. Buchwald, B. C. Edwards, T. R. Gosnell, and C. E. Mungan, "Observation of laser-induced fluorescent cooling of a solid," Nature **377**, 500–503 (1995).
9. S. D. Melgaard, D. V. Seletskiy, A. D. Lieto, M. Tonelli, and M. Sheik-Bahae, "Optical refrigeration to 119 K, below National Institute of Standards and Technology cryogenic temperature," Opt. Lett. **38**, 1588–1590 (2013).
10. P. B. Roder, B. E. Smith, X. Zhou, M. J. Crane, and P. J. Pauzauskie, "Laser refrigeration of hydrothermal nanocrystals in physiological media," Proc. Natl. Acad. Sci. USA **112**, 15024–15029 (2015).
11. A. T. M. A. Rahman and P. F. Barker, "Laser refrigeration, alignment and rotation of levitated Yb^{3+}:YLF nanocrystals," Nat. Photonics **11**, 634–638 (2017).
12. Q. Lin, J. Rosenberg, X. Jiang, K. J. Vahala, and O. Painter, "Mechanical oscillation and cooling actuated by the optical gradient force," Phys. Rev. Lett. **103**, 103601 (2009).
13. G. S. Wiederhecker, L. Chen, A. Gondarenko, and M. Lipson, "Controlling photonic structures using optical forces," Nature **462**, 633–636 (2009).
14. M. Aspelmeyer, T. J. Kippenberg, and F. Marquardt, "Cavity optomechanics," Rev. Mod. Phys. **86**, 1391–1452 (2014).
15. A. Derevianko and H. Katori, "Colloquium: physics of optical lattice clocks," Rev. Mod. Phys. **83**, 331–347 (2011).

16. W. Ren, T. Li, Q. Qu, B. Wang, L. Li, D. Lü, W. Chen, and L. Liu, "Development of a space cold atom clock," Natl. Sci. Rev. **7**, 1828–1836 (2020).
17. B. Chen, J. Long, H. Xie, C. Li, L. Chen, B. Jiang, and S. Chen, "Portable atomic gravimeter operating in noisy urban environments," Chin. Opt. Lett. **18**, 090201 (2020).
18. C. L. Degen, F. Reinhard, and P. Cappellaro, "Quantum sensing," Rev. Mod. Phys. **89**, 035002 (2017).
19. J. Dalibard, F. Gerbier, G. Juzeliūnas, and P. Öhberg, "Colloquium: artificial gauge potentials for neutral atoms," Rev. Mod. Phys. **83**, 1523–1543 (2011).
20. R. A. Hart, P. M. Duarte, T.-L. Yang, X. Liu, T. Paiva, E. Khatami, R. T. Scalettar, N. Trivedi, D. A. Huse, and R. G. Hulet, "Observation of antiferromagnetic correlations in the Hubbard model with ultracold atoms," Nature **519**, 211–214 (2015).
21. H. Bernien, S. Schwartz, A. Keesling, H. Levine, A. Omran, H. Pichler, S. Choi, A. S. Zibrov, M. Endres, M. Greiner, V. Vuletić, and M. D. Lukin, "Probing many-body dynamics on a 51-atom quantum simulator," Nature **551**, 579–584 (2017).
22. K. Hammerer, A. S. Sørensen, and E. S. Polzik, "Quantum interface between light and atomic ensembles," Rev. Mod. Phys. **82**, 1041–1093 (2010).
23. M. Saffman, T. G. Walker, and K. Mølmer, "Quantum information with Rydberg atoms," Rev. Mod. Phys. **82**, 2313–2363 (2010).
24. D. S. Weiss, E. Riis, Y. Shevy, P. J. Ungar, and S. Chu, "Optical molasses and multilevel atoms: experiment," J. Opt. Soc. Am. B **6**, 2072–2083 (1989).
25. R. Gati, B. Hemmerling, J. Fölling, M. Albiez, and M. K. Oberthaler, "Noise thermometry with two weakly coupled Bose-Einstein condensates," Phys. Rev. Lett. **96**, 130404 (2006).
26. F. M. Spiegelhalder, A. Trenkwalder, D. Naik, G. Hendl, F. Schreck, and R. Grimm, "Collisional stability of 40 K immersed in a strongly interacting Fermi gas of ^{6}Li," Phys. Rev. Lett. **103**, 223203 (2009).
27. H. Cheng, S. Deng, Z. Zhang, J. Xiang, J. Ji, W. Ren, T. Li, Q. Qu, L. Liu, and D. Lü, "Uncertainty evaluation of the second-order Zeeman shift of a transportable ^{87}Rb atomic fountain clock," Chin. Opt. Lett. **19**, 120201 (2021).
28. X. Wang, Y. Sun, H.-D. Cheng, J.-Y. Wan, Y.-L. Meng, L. Xiao, and L. Liu, "Nearly nondestructive thermometry of labeled cold atoms and application to isotropic laser cooling," Phys. Rev. Appl. **14**, 024030 (2020).
29. X. Wang, Y. Sun, and L. Liu, "Characterization of isotropic laser cooling for application in quantum sensing," Opt. Express **29**, 43435–43444 (2021).
30. P. G. Petrov, D. Oblak, C. L. G. Alzar, N. Kjærgaard, and E. S. Polzik, "Nondestructive interferometric characterization of an optical dipole trap," Phys. Rev. A **75**, 033803 (2007).
31. M. Mehboudi, A. Lampo, C. Charalambous, L. A. Correa, M. A. García-March, and M. Lewenstein, "Using polarons for sub-nK quantum nondemolition thermometry in a Bose-Einstein condensate," Phys. Rev. Lett. **122**, 030403 (2019).
32. J. C. Maxwell, *Theory of Heat* (Longman, 1871).
33. V. Serreli, C.-F. Lee, E. R. Kay, and D. A. Leigh, "A molecular information ratchet," Nature **445**, 523–527 (2007).
34. S. Toyabe, T. Sagawa, M. Ueda, E. Muneyuki, and M. Sano, "Experimental demonstration of information-to-energy conversion and validation of the generalized Jarzynski equality," Nat. Phys. **6**, 988–992 (2010).
35. J. V. Koski, V. F. Maisi, T. Sagawa, and J. P. Pekola, "Experimental observation of the role of mutual information in the nonequilibrium dynamics of a Maxwell demon," Phys. Rev. Lett. **113**, 030601 (2014).
36. J. V. Koski, V. F. Maisi, J. P. Pekola, and D. V. Averin, "Experimental realization of a Szilard engine with a single electron," Proc. Natl. Acad. Sci. USA **111**, 13786–13789 (2014).
37. J. V. Koski, A. Kutvonen, I. M. Khaymovich, T. Ala-Nissila, and J. P. Pekola, "On-chip Maxwell's demon as an information-powered refrigerator," Phys. Rev. Lett. **115**, 260602 (2015).
38. M. D. Vidrighin, O. Dahlsten, M. Barbieri, M. S. Kim, V. Vedral, and I. A. Walmsley, "Photonic Maxwell's demon," Phys. Rev. Lett. **116**, 050401 (2016).
39. P. A. Camati, J. P. S. Peterson, T. B. Batalhão, K. Micadei, A. M. Souza, R. S. Sarthour, I. S. Oliveira, and R. M. Serra, "Experimental rectification of entropy production by Maxwell's demon in a quantum system," Phys. Rev. Lett. **117**, 240502 (2016).
40. N. Cottet, S. Jezouin, L. Bretheau, P. Campagne-Ibarcq, Q. Ficheux, J. Anders, A. Auffèves, R. Azouit, P. Rouchon, and B. Huard, "Observing a quantum Maxwell demon at work," Proc. Natl. Acad. Sci. USA **114**, 7561–7564 (2017).
41. R. Sánchez, J. Splettstoesser, and R. S. Whitney, "Nonequilibrium system as a demon," Phys. Rev. Lett. **123**, 216801 (2019).
42. T. Binnewies, U. Sterr, J. Helmcke, and F. Riehle, "Cooling by Maxwell's demon: preparation of single-velocity atoms for matter-wave interferometry," Phys. Rev. A **62**, 011601 (2000).
43. J. J. Thorn, E. A. Schoene, T. Li, and D. A. Steck, "Dynamics of cold atoms crossing a one-way barrier," Phys. Rev. A **79**, 063402 (2009).
44. L. Liu, D.-S. Lü, W.-B. Chen, T. Li, Q.-Z. Qu, B. Wang, L. Li, W. Ren, Z.-R. Dong, J.-B. Zhao, W.-B. Xia, X. Zhao, J. W. Ji, M.-F. Ye, Y.-G. Sun, Y.-Y. Yao, D. Song, Z.-G. Liang, S.-J. Hu, D.-H. Yu, X. Hou, W. Shi, H.-G. Zang, J.-F. Xiang, X.-K. Peng, and Y.-Z. Wang, "In-orbit operation of an atomic clock based on laser-cooled ^{87}Rb atoms," Nat. Commun. **9**, 2760 (2018).
45. G. M. Tino, A. Bassi, G. Bianco, K. Bongs, P. Bouyer, L. Cacciapuoti, S. Capozziello, X. Chen, M. L. Chiofalo, A. Derevianko, W. Ertmer, N. Gaaloul, P. Gill, P. W. Graham, J. M. Hogan, L. Iess, M. A. Kasevich, H. Katori, C. Klempt, X. Lu, L.-S. Ma, H. Müller, N. R. Newbury, C. W. Oates, A. Peters, N. Poli, E. M. Rasel, G. Rosi, A. Roura, C. Salomon, S. Schiller, W. Schleich, D. Schlippert, F. Schreck, C. Schubert, F. Sorrentino, U. Sterr, J. W. Thomsen, G. Vallone, F. Vetrano, P. Villoresi, W. von Klitzing, D. Wilkowski, P. Wolf, J. Ye, N. Yu, and M. Zhan, "SAGE: a proposal for a space atomic gravity explorer," Eur. Phys. J. D **73**, 228 (2019).
46. Y. Z. Wang, "Atomic beam slowing by diffusive light in an integrating sphere," in *Proceedings of the National Symposium on Frequency Standards* (1979).
47. W. Ketterle, A. Martin, M. A. Joffe, and D. E. Pritchard, "Slowing and cooling atoms in isotropic laser light," Phys. Rev. Lett. **69**, 2483–2486 (1992).
48. H. Batelaan, S. Padua, D. H. Yang, C. Xie, R. Gupta, and H. Metcalf, "Slowing of ^{87}Rb atoms with isotropic light," Phys. Rev. A **49**, 2780–2784 (1994).
49. M. Langlois, L. De Sarlo, D. Holleville, N. Dimarcq, J.-F. Schaff, and S. Bernon, "Compact cold-atom clock for onboard timebase: tests in reduced gravity," Phys. Rev. Appl. **10**, 064007 (2018).
50. E. Guillot, P.-E. Pottie, and N. Dimarcq, "Three-dimensional cooling of cesium atoms in a reflecting copper cylinder," Opt. Lett. **26**, 1639–1641 (2001).
51. H. J. Metcalf and P. van der Straten, *Laser Cooling and Trapping* (Springer-Verlag, 1999).
52. X.-C. Wang, H.-D. Cheng, L. Xiao, B.-C. Zheng, Y.-L. Meng, L. Liu, and Y.-Z. Wang, "Measurement of spatial distribution of cold atoms in an integrating sphere," Chin. Phys. Lett. **29**, 023701 (2012).
53. S. Trémine, E. de Clercq, and P. Verkerk, "Isotropic light versus six-beam molasses for Doppler cooling of atoms from background vapor: theoretical comparison," Phys. Rev. A **96**, 023411 (2017).
54. F.-X. Esnault, D. Holleville, N. Rossetto, S. Guerandel, and N. Dimarcq, "High-stability compact atomic clock based on isotropic laser cooling," Phys. Rev. A **82**, 033436 (2010).
55. P. Liu, Y. Meng, J. Wan, X. Wang, Y. Wang, L. Xiao, H. Cheng, and L. Liu, "Scheme for a compact cold-atom clock based on diffuse laser cooling in a cylindrical cavity," Phys. Rev. A **92**, 062101 (2015).
56. Y. Wang, Y. Meng, J. Wan, M. Yu, X. Wang, L. Xiao, H. Cheng, and L. Liu, "Optical-plus-microwave pumping in a magnetically insensitive state of cold atoms," Phys. Rev. A **97**, 023421 (2018).
57. W. D. Phillips, "Nobel lecture: laser cooling and trapping of neutral atoms," Rev. Mod. Phys. **70**, 721–741 (1998).
58. H. Metcalf, "Entropy exchange in laser cooling," Phys. Rev. A **77**, 061401 (2008).